PHYSICAL REVIEW B **72**, 165204 (2005)

Prospects for high temperature ferromagnetism in (Ga,Mn)As semiconductors

T. Jungwirth,[1,2] K. Y. Wang,[2] J. Mašek,[3] K. W. Edmonds,[2] Jürgen König,[4] Jairo Sinova,[5] M. Polini,[6] N. A. Goncharuk,[1] A. H. MacDonald,[7] M. Sawicki,[8] A. W. Rushforth,[2] R. P. Campion,[2] L. X. Zhao,[2] C. T. Foxon,[2] and B. L. Gallagher[2]

[1]*Institute of Physics ASCR, Cukrovarnická 10, 162 53 Praha 6, Czech Republic*
[2]*School of Physics and Astronomy, University of Nottingham, Nottingham NG7 2RD, United Kingdom*
[3]*Institute of Physics ASCR, Na Slovance 2, 182 21 Praha 8, Czech Republic*
[4]*Institut für Theoretische Physik III, Ruhr-Universität Bochum, 44780 Bochum, Germany*
[5]*Department of Physics, Texas A&M University, College Station, Texas 77843-4242, USA*
[6]*NEST-INFM and Scuola Normale Superiore, I-56126 Pisa, Italy*
[7]*Department of Physics, University of Texas at Austin, Austin, Texas 78712-1081, USA*
[8]*Institute of Physics, Polish Academy of Sciences, 02668 Warszawa, Poland*

(Received 9 May 2005; revised manuscript received 21 July 2005; published 13 October 2005)

We report on a comprehensive combined experimental and theoretical study of Curie temperature trends in (Ga,Mn)As ferromagnetic semiconductors. Broad agreement between theoretical expectations and measured data allows us to conclude that T_c in high-quality metallic samples increases linearly with the number of uncompensated local moments on Mn_{Ga} acceptors, with no sign of saturation. Room temperature ferromagnetism is expected for a 10% concentration of these local moments. Our magnetotransport and magnetization data are consistent with the picture in which Mn impurities incorporated during growth at interstitial Mn_I positions act as double-donors and compensate neighboring Mn_{Ga} local moments because of strong near-neighbor Mn_{Ga}—Mn_I antiferromagnetic coupling. These defects can be efficiently removed by post-growth annealing. Our analysis suggests that there is no fundamental obstacle to substitutional Mn_{Ga} doping in high-quality materials beyond our current maximum level of 6.8%, although this achievement will require further advances in growth condition control. Modest charge compensation does not limit the maximum Curie temperature possible in ferromagnetic semiconductors based on (Ga,Mn)As.

DOI: 10.1103/PhysRevB.72.165204 PACS number(s): 75.50.Pp, 75.30.Gw, 73.61.Ey

I. INTRODUCTION

After some frustration in the community caused by the difficulties encountered in overcoming the apparent Curie temperature limit in (Ga,Mn)As of $T_c=110$ K,[1–4] the record transition temperature has been steadily increasing over the last two years.[5–9] The maximum $T_c=173$ K reported[9] to date is likely another short-lived record in bulk (Ga,Mn)As ferromagnets. It is now established that the success has been made possible by the technological progress in controlling crystallographic quality of the materials, namely, in reducing the number of unintentional charge and moment compensating defects through optimized growth and post-growth annealing procedures.[3–10] Experiments also suggest that the general picture of ferromagnetism that applies to these metallic (Ga,Mn)As systems is the one in which magnetic coupling between local Mn moments is mediated by delocalized holes in the (Ga,Mn)As valence band. The fact that the mechanism does not imply a fundamental T_c limit below room temperature motivates a detailed analysis of our understanding of the T_c trends in currently available high quality metallic materials with Mn doping ranging from approximately 2% to 9%.

Curie temperatures in metallic (Ga,Mn)As have been studied theoretically starting from semiphenomenological[11–15] and microscopic models[16–21] of the electronic structure. The former approach asserts a localized character of the five Mn_{Ga} d orbitals forming a moment $S=5/2$ and describes hole states in the valence band using the Kohn-Luttinger parameterization for GaAs (Ref. 22) and a single constant J_{pd} which characterizes the exchange interaction between Mn_{Ga} and hole spins. The exchange interaction follows from hybridization between Mn d orbitals and valence band p orbitals. The semiphenomenological Hamiltonian implicitly assumes that a canonical transformation has been performed which eliminated the hybridization.[21] In this approach the hybridization is implicitly assumed to be weak in several different ways, and the canonical transformation ignored in representing observables. Although this approach is consistent, it should be realized that the localized d orbitals in the phenomenological Hamiltonian are in reality hybridized with the valence band.

The advantage of the semiphenomenological approach is that it uses the experimental value[23,24] for $J_{pd}=54\pm9$ meV nm^3, i.e., it correctly captures the strength of the magnetic interaction that has been established to play the key role in ferromagnetism in (Ga,Mn)As. The model also accounts for strong spin-orbit interaction present in the host valence band which splits the three p bands into a heavy-hole, light-hole, and a split-off band with different dispersions. The spin-orbit coupling is not only responsible for a number of distinct magnetic[25–28] and magneto-transport[29–32] properties of (Ga,Mn)As ferromagnets but the resulting complexity of the valence band was shown[14,33] to play also an important role in suppressing magnetization fluctuation effects and, therefore, stabilizing the ferromagnetic state itself. On the other hand, describing the potentially complex behavior of Mn_{Ga} in GaAs by a single parameter may oversimplify the problem. The calculations omit, for example, the contribution of direct antiferromagnetic superexchange to the cou-

pling of near-neighbor Mn pairs, and the whole model inevitably breaks down if valence fluctuations of Mn_{Ga} *d* electrons become strong.

Microscopic theories, whether based on the tight-binding-approximation (TBA) parameterization of energies and overlaps of valence orbitals in the lattice[20,21] or on the *ab initio* local-density-approximation (LDA) schemes,[16–19] make no assumption upon the character of Mn_{Ga} impurities in GaAs and their magnetic coupling. They are therefore useful for studying material trends in T_c as a function of Mn doping or density and position in the lattice of other intentional or unintentional impurities present in real systems.[34] Because spin-orbit interactions add to the numerical complexity of calculations that are already challenging, they have normally been neglected. Another shortcoming of the *ab initio* approaches is the incomplete elimination of self-interaction effects which leads to smaller relative displacement of the Mn *d* levels and the top of the valence band. This results in an overestimated strength of the *p-d* exchange as compared to experiment.

Within the mean-field approximation, which considers thermodynamics of an isolated Mn moment in an effective field and neglects correlated Mn—Mn fluctuations, microscopic calculations[18] typically yield larger T_c's than the semiphenomenological models[13,14] that use the experimental J_{pd} value. Stronger *p-d* exchange in the microscopic theories leads, however, also to a larger suppression of the Curie temperature due to fluctuation effects, especially so in highly doped systems.[18] (A closer agreement in the character of the T_c vs Mn-doping curves, calculated within the two formalisms, is obtained when the deficiencies of density-functional theories are partly eliminated by introducing a correlation energy constant within the LDA+U schemes.[18]) Despite the above weaknesses of semiphenomenological and microscopic calculations, an overall, qualitatively consistent picture is clearly emerging from these complementary theoretical approaches that, as we discuss below, provides a useful framework for analyzing measured T_c's.

In experimental Curie temperature studies it is crucial to decouple intrinsic properties of (Ga,Mn)As ferromagnets from extrinsic, effects due to the presence of unintentional impurities. Arsenic antisites (As_{Ga}) and interstitial manganese (Mn_I) represent two major sources of charge compensation in (Ga,Mn)As grown by low-temperature molecular beam epitaxy (LT-MBE), both acting as double-donors.[35,36] A Mn_I cation when attracted to a Mn_{Ga} anion compensates also the Mn_{Ga} local moment as the two species are expected to couple antiferromagnetically[8,37,38] due to superexchange over the whole range from strong to weak charge compensation.

The As_{Ga} antisites are stable[39] up to $\sim$450 °C, which is well above the transition temperature from a uniform diluted magnetic semiconductor to a multiphase structure with metallic MnAs and other precipitates. Therefore, the number of As_{Ga} defects has to be minimized already during the LT-MBE growth by precisely controlling the stoichiometry of deposited epilayers.[40] The Mn_I impurity concentration can be significant in as-grown structures. These defects are, however, much more mobile than the As antisites. During annealing at temperatures close to the MBE growth temperature $\sim$200 °C they out-diffuse and are passivated at the epilayer surface.[8]

In this paper we have collected data for a set of samples that show very weak charge and moment compensation after annealing, i.e., a negligible number of As_{Ga}, which allows us to determine experimentally T_c trends related to intrinsic properties of (Ga,Mn)As ferromagnets. We also point out that conclusions made here are based on magnetic and transport measurements in 16 different (Ga,Mn)As materials (8 as-grown and 8 annealed) which we fabricated and analyzed using consistent experimental procedures and which, therefore, represent a unique comprehensive set of measurements. A direct quantitative comparison with results obtained by other groups[1,2,4,6,7,10] is hindered by incompatabilities in the employed growth and characterization techniques. Nevertheless, the behavior of materials synthetized in different laboratories clearly follows similar patterns for Mn doping up to $\sim$5%. In samples with higher Mn content the levels and nature of compensating defects can vary more strongly from material to material depending on the details of the growth and post-growth annealing procedures. This may explain large differences in conductivities and Curie temperatures reported by different groups in highly doped (Ga,Mn)As materials.

The paper is organized as follows: In Sec. II we start with the semiphenomenological mean-field approximation (Sec. II A) to set up a scale of expected Curie temperatures in the material, assuming homogeneous distribution of Mn_{Ga} ions (the virtual-crystal approximation). We then discuss various physically distinct effects that are not captured by this picture. In Sec. II B we evaluate the Stoner enhancement of the Curie temperature due to hole-hole exchange interaction. Suppression of T_c due to antiferromagnetic superexchange contribution to the near-neighbor Mn_{Ga}—Mn_{Ga} coupling in highly compensated samples[41] is illustrated in Sec. II C. In this section we discuss also effects on T_c arising from the discreteness of random Mn_{Ga} positions in the lattice that becomes important in the opposite regime, i.e., in systems with low charge compensation or co-doped with additional nonmagnetic acceptors. Effects beyond the mean-field approximation, namely the disappearance of the ferromagnetic long-range order due to collective Mn_{Ga} moments fluctuations are discussed in Sec. II D. Since the Mn_{Ga}, Mn_I, and hole densities represent key parameters in the discussion of measured Curie temperatures, we present in Sec. II E theoretical predictions for equilibrium partial concentrations of substitutional Mn_{Ga} and interstitial Mn_I impurities in as-grown samples, and in Sec. II F we estimate the accuracy of the Hall measurement of hole density in the polarized (Ga,Mn)As valence bands.

Measured T_c and hole densities are presented in Sec. III A for a set of samples with different nominal Mn doping, before and after annealing. Motivated by the above theoretical analysis we determine in Sec. III B the partial density of Mn_{Ga} and Mn_I, and the effective density of uncompensated Mn_{Ga} local moments in our samples. The interpretation is based on total Mn-doping values, obtained from secondary ion mass spectroscopy (SIMS), and Hall measurements of the hole densities before and after annealing. Consistency of these results is checked by comparisons with independent

magnetization measurements. In Sec. III C we present experimental T_c dependencies on uncompensated Mn_{Ga} moment and hole densities and compare the data with theory predictions. Technological issues related to the growth of (Ga,Mn)As epilayers with large Mn concentrations are discussed in Sec. IV. Our perspective on high-temperature ferromagnetism in (Ga,Mn)As semiconductors is summarized in Sec. V.

II. THEORY

A. Mean-field virtual crystal approximation

The description of ordered states in (Ga,Mn)As is greatly simplified by the virtual-crystal approximation in which the random Mn_{Ga} distribution is replaced by a continuum with the same average local moment density and the role of other defects is neglected, apart from the potential hole or moment compensation.[11,12,42,43] Microscopic TBA calculations showed[20] very little effect of positional disorder on the strength of magnetic couplings in (Ga,Mn)As epilayers with metallic conductivities of interest here, which partly justifies the virtual-crystal approach. Other detailed theoretical studies, corroborated by experimental data below, confirm the absence of any significant magnetic frustration in this ferromagnetic semiconductor associated with the random positions of Mn_{Ga} moments in the lattice.[44,45]

In the mean-field approximation,[11,12] each local Mn_{Ga} moment is described by a Hamiltonian $\vec{S}_I \cdot \vec{H}_{MF}$ where $\vec{S}_I$ is the Mn_{Ga} local spin operator, $\vec{H}_{MF}=J_{pd}\langle\vec{s}\rangle$, and $\langle\vec{s}\rangle$ is the mean spin density of the valence band holes. H_{MF} is an effective field seen by the local moments due to spin polarization of the band holes, analogous to the nuclear Knight shift. Similarly $\vec{h}_{MF}=J_{pd}N_{Mn}\langle\vec{S}\rangle$ is an effective magnetic field experienced by the valence band holes, where $\langle\vec{S}\rangle$ is the mean spin polarization of the Mn_{Ga} local moments, and $N_{Mn}=4x/a_{lc}^3$ is the Mn_{Ga} density in $Ga_{1-x}Mn_xAs$ with a lattice constant a_{lc}. The dependence of $\langle\vec{S}\rangle$ on temperature and field H_{MF} is given[43] by the Brillouin function:

$$\langle\vec{S}\rangle = \frac{\vec{H}_{MF}}{|H_{MF}|} S B_s(S|H_{MF}|/k_B T). \tag{1}$$

The Curie temperature is found by linearizing H_{MF} and B_s around $\langle\vec{S}\rangle=0$:

$$\vec{H}_{MF} \approx J_{pd}^2 N_{Mn}\langle\vec{S}\rangle\chi_f$$

$$B_s \approx \frac{S+1}{3}\frac{S|H_{MF}|}{k_B T_c}. \tag{2}$$

Here χ_f is the itinerant hole spin susceptibility given by

$$\chi_f = \frac{d\langle s\rangle}{dh_{MF}} = -\frac{d^2 e_T}{dh_{MF}^2}, \tag{3}$$

and e_T is the total energy per volume of the holes. Equations (1) and (2) give

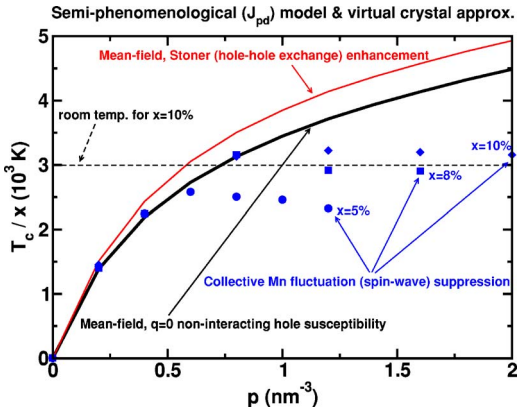

FIG. 1. (Color online) Ferromagnetic transition temperatures of (Ga,Mn)As calculated within the effective Hamiltonian and virtual-crystal approximation: mean-field (thick black line), Stoner enhancement of T_c (thin line), spin-wave suppression of T_c (closed diamonds, squares, and circles).

$$k_B T_c = \frac{N_{Mn} S(S+1)}{3} J_{pd}^2 \chi_f. \tag{4}$$

Qualitative implications of this T_c Eq. (4) can be understood within a model itinerant hole system with a single spin-split band and an effective mass m^*. The kinetic energy contribution e_k to the total energy of the band holes gives a susceptibility:

$$\chi_{f,k} = -\frac{d^2 e_k}{dh_{MF}^2} = \frac{m^* k_F}{4\pi^2\hbar^2}, \tag{5}$$

where k_F is the Fermi wave vector. Within this approximation T_c is proportional to the Mn_{Ga} density, to the hole Fermi wave vector, i.e., to $p^{1/3}$ where p is the hole density, and to the hole effective mass m^*.

To obtain quantitative predictions for the critical temperature, it is necessary to evaluate the itinerant hole susceptibility using a realistic band Hamiltonian, $H=H_{KL}+\vec{s}\cdot\vec{h}_{MF}$, where H_{KL} the six-band Kohn-Luttinger model of the GaAs host band[22] and $\vec{s}$ is the hole spin operator.[12,25,26] The results, represented by the solid black line in Fig. 1, are consistent with the qualitative analysis based on the parabolic band model, i.e., T_c follows roughly the $\sim xp^{1/3}$ dependence. Based on these calculations, room temperature ferromagnetism in (Ga,Mn)As is expected for 10% Mn_{Ga} doping in weakly compensated samples.

B. Stoner enhancement of T_c

In highly doped (Ga,Mn)As epilayers the hole-hole correlation effects are weak and can be neglected. The exchange total energy e_x adds a contribution to the hole spin susceptibility:

$$\chi_{f,x} = -\frac{d^2 e_x}{dh_{MF}^2}, \tag{6}$$

which for a single parabolic spin-split band reads,

$$\chi_{f,x} = \frac{e^2 (m^*)^2}{4\pi^3 \varepsilon \hbar^4}, \tag{7}$$

where ε is the dielectric constant of the host semiconductor. Equation (7) suggests a hole-density independent Stoner enhancement of T_c proportional to Mn_{Ga} concentration and $(m^*)^2$.

As in the noninteracting hole case discussed above, the detailed valence-band structure has to be accounted for to make quantitative estimates of the Stoner T_c enhancement. The red line in Fig. 1 shows the Stoner T_c enhancement calculated numerically from Eqs. (6). As expected, T_c stays roughly proportional to $xp^{1/3}$ even if hole-hole exchange interactions are included, and the enhancement of the Curie temperature due to interactions is of the order $\sim$10–20 %.

C. Discreteness of random Mn_{Ga} positions, superexchange

So far, the mean-field analysis of T_c has neglected discreteness in random Mn_{Ga} positions in the lattice and other magnetic coupling mechanisms; besides the kinetic-exchange, this includes the near-neighbor superexchange. The former point can be expected to affect T_c at large hole densities, i.e., when the hole Fermi wavelength approaches inter-atomic distances. In the opposite limit of strongly compensated systems, where the overall magnitude of the hole-mediated exchange is weaker, antiferromagnetic superexchange can dominate the near-neighbor Mn_{Ga}—Mn_{Ga} coupling,[41] leading to a reduced Curie temperature.[18,20] This type of magnetic interaction was ignored in the previous section. We emphasize that the phenomenological model cannot be applied consistently when nearest-neighbor interactions dominate, since it implicitly assumes that all length scales are longer than a lattice constant. We also note that net antiferromagnetic coupling of near-neighbor Mn_{Ga}—Mn_{Ga} pairs is expected only in systems with large charge compensations. In weakly compensated (Ga,Mn)As the ferromagnetic contribution takes over.[41,46]

Besides the above effects of random Mn distribution, Mn positional disorder can directly modify the *p-d* interaction when the coherence of Bloch states becomes significantly disturbed. Microscopic theories, such as the TBA calculations[20] presented in this section or approaches based on *ab initio* LDA band structure,[18] capture all these effects on an equal footing and can be used to estimate trends in mean-field T_c beyond the virtual-crystal approximation. The theories do not assert any specific magnetic coupling mechanism from the outset. Instead, these follow from the microscopic description of the electronic structure of the doped crystal.

Within the coherent-potential approximation (CPA), disorder effects appear in the finite spectral width of hole quasiparticle states. Since realizations with near-neighbor Mn_{Ga} ions are included within the disorder-averaged TBA/CPA with the proper statistical probability, short-range local moment interactions (such as superexchange) contribute to the final magnetic state.

The parametrization of our TBA Hamiltonian was chosen to provide the correct band gap for a pure GaAs crystal[47] and the appropriate exchange splitting of the Mn *d* states. Local changes of the crystal potential at Mn_{Ga}, represented by shifted atomic levels, are estimated using Ref. 48. Long-range tails of the impurity potentials, which become less important with increasing level of doping, are neglected. (Note, that the Thomas-Fermi screening length is only 3–5 Å for typical carrier densities,[49] i.e., comparable to the lattice constant.) Also lattice relaxation effects are neglected within the CPA.

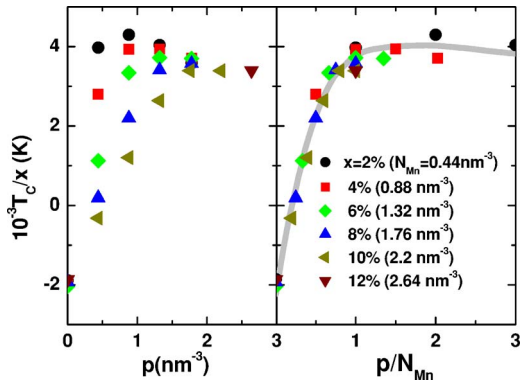

FIG. 2. (Color online) T_c calculations within the microscopic TBA/CPA model: T_c vs hole density (left panel), T_c vs number of holes per Mn_{Ga} (right panel). The overall theoretical T_c trend is highlighted in gray to facilitate comparison with experimental data discussed in Sec. III C.

In our TBA/CPA calculations, hole density is varied independently of Mn_{Ga} doping by adding nonmagnetic donors (Si or Se) or acceptors (C or Be). The resulting valence-band splitting is almost independent of the density of these nonmagnetic impurities at fixed N_{Mn}, which indicates that quasiparticle broadening due to positional disorder has only a weak effect on the strength of the kinetic-exchange coupling. We intentionally did not use Mn_I donors in these calculations to avoid mixing of the (arguably) most important effect of this defect which is moment compensation. This is discussed separately in Sec. II E.

The TBA/CPA Curie temperatures are obtained using the compatibility of the model with the Weiss mean-field theory. The strength of the Mn_{Ga}—Mn_{Ga} coupling is characterized by the energy cost of flipping one Mn_{Ga} moment, which can be calculated for a given chemical composition.[50] This effective field H_{eff} corresponds to H_{MF} in the semi-phenomenological kinetic-exchange model used in the previous section, i.e.,

$$k_B T_c = \frac{S+1}{3} H_{eff}. \tag{8}$$

In Fig. 2 we plot the mean-field TBA/CPA transition temperatures as a function of hole densities for several Mn_{Ga} concentrations. Since the typical T_c's here are similar to those in Fig. 1 we can identify, based on the comparison between the two figures, the main physical origins of the deviations from the $T_c \sim xp^{1/3}$ trend. Closed circles in the left panel of Fig. 2, which correspond to a relatively low local Mn_{Ga} moment concentration (x=2%) and hole densities

ranging up to $p=4N_{\mathrm{Mn}}$, show the expected supression of T_c at large p. The effect of superexchange in the opposite limit is clearly seen when inspecting, e.g., the $x=10\%$ data for $p<1$ nm^{-3}. The mean-field TBA/CPA Curie temperature is largely suppressed here or even negative, meaning that the ferromagnetic state becomes unstable due to the short-range antiferromagnetic coupling. Also, the inhomogeneity of the carrier distribution in the disordered mixed crystal may contribute to the steep decrease of T_c with increasing compensation. Although the Curie temperatures in the left panel of Fig. 2 appear to depart strongly for the $T_c \sim xp^{1/3}$ dependence, the linearity with x is almost fully recovered when T_c is plotted as a function of the number of holes per $\mathrm{Mn_{Ga}}$, p/N_{Mn} (see right panel of Fig. 2). Note that for compensations $(1-p/N_{\mathrm{Mn}})$ reaching 100% this property of the superexchange coupling is reminiscent of the behavior of (II,Mn)VI diluted magnetic semiconductors[51] in which Mn acts as an isovalent magnetic impurity. The dependence on p in (Ga,Mn)As is expected to become very weak, however, when reaching the uncompensated limit or when further increasing hole density by nonmagnetic acceptor co-doping.

D. Collective Mn-moment fluctuations

The potential importance of correlated Mn-moment fluctuations on T_c in (Ga,Mn)As can be illustrated by recalling, within a simple parabolic band model, the RKKY (or Friedel) oscillations effect which occurs as a consequence of the $2k_F$ anomaly in the wave vector dependent susceptibility of the hole system.[14,42] In this picture, the sign of the indirect kinetic-exchange $\mathrm{Mn_{Ga}}$—$\mathrm{Mn_{Ga}}$ coupling fluctuates as $\cos(2k_F d)$, where d is the distance between $\mathrm{Mn_{Ga}}$ moments, and its amplitude decays as d^3. We can estimate the average $\mathrm{Mn_{Ga}}$—$\mathrm{Mn_{Ga}}$ separation in a (Ga,Mn)As random alloy as $\bar{d}=2(3/4\pi N_{\mathrm{Mn}})^{1/3}$. If the spin-orbit interaction and band-warping are neglected, the top of the valence band is formed by six degenerate parabolic bands with $k_F=(\pi^2 p)^{1/3}$. For uncompensated (Ga,Mn)As systems ($p=N_{\mathrm{Mn}}$), we then obtain $\cos(2k_F\bar{d})\approx -1$ which means that the role of these fluctuations cannot be generally discarded. In realistic valence bands, as we see below, the fluctuations are suppressed due to nonparabolic and anisotropic dispersions of the heavy-and light-hole bands and due to the strong spin-orbit coupling.

On a more quantitative level, we can establish the range of reliability and estimate corrections to the mean-field theory in (Ga,Mn)As by accounting for the suppression of the Curie temperature within quantum theory of long-wavelength spin waves in the semiphenomenological virtual-crystal model. We note that a qualitatively similar picture is obtained using Monte Carlo simulations which treat Mn-moments as classical variables and account for positional disorder.[14,43,52] Isotropic ferromagnets have spin-wave Goldstone collective modes whose energies vanish at long wavelengths,

$$\Omega_k = Dk^2 + \mathcal{O}(k^4), \tag{9}$$

where k is the wave vector of the mode. Spin-orbit coupling breaks rotational symmetry and leads to a finite gap. According to numerical studies,[33] this gap is small however, much smaller than $k_B T_c$, for example, and plays a role in magnetic fluctuations only at very low temperatures. Spin-wave excitations reduce the total spin by one, at an energy cost that is, at least at long wavelengths, much smaller than the mean-field value, H_{MF}. The importance of these correlated spin excitations, neglected by mean-field theory, can be judged by evaluating an approximate T_c bound based on the following argument which uses a Debye-like model for the magnetic excitation spectrum. When spin-wave interactions are neglected, the magnetization vanishes at the temperature where the number of excited spin waves equals the total spin of the ground state:

$$N_{\mathrm{Mn}} S = \frac{1}{2\pi^2}\int_0^{k_D} dk\, k^2 n(\Omega_k), \tag{10}$$

where $n(\Omega_k)$ is the Bose occupation number and the Debye cutoff, $k_D=(6\pi^2 N_{\mathrm{Mn}})^{1/3}$. It follows that the ferromagnetic transition temperature cannot exceed

$$k_B T_c = \frac{2S+1}{6} k_D^2 D(T_c). \tag{11}$$

In applying this formula to estimate T_c we have approximated the temperature dependence of the spin stiffness by

$$D(T) = D_0 \langle S\rangle(T)/S, \tag{12}$$

where D_0 is the zero-temperature stiffness,[33,53] and $\langle S\rangle(T)$ is the mean-field Mn polarization[26] at temperature T. If the difference between T_c obtained from the self-consistent solution of Eqs. (11) and (12) and the mean-field Curie temperature in Eq. (4) is large, the typical local valence-band carrier polarization will remain finite above the critical temperature and the ferromagnetism will disappear only because of the loss of long-range spatial order; for example, the usual circumstance for transition metal ferromagnetism.

In discussing corrections to mean-field-theory T_c estimates, we compare spin-stiffness results obtained with the simple two-band and realistic six-band models. Details on the formalism used to calculate D_0 can be found in Refs. 33 and 54. We find that the zero-temperature spin stiffness is always much larger in the six-band model. For (Ga,Mn)As, the two-band model underestimates D_0 by a factor of $\sim 10-30$ over the range of hole densities considered. Furthermore, the trend is different: in the two-band model the stiffness decreases with increasing density, while for the six-band description the initial increase is followed by a saturation. Even in the limit of low carrier concentrations, it is not only the (heavy-hole) mass of the lowest band which is important for the spin stiffness. In the realistic band model, heavy-holes have their spin and orbital angular momenta aligned approximately along the direction of the Bloch wave vector. Exchange interactions with Mn spins mix the heavy holes with more dispersive light holes. The calculations show that heavy-light mixing is responsible for the relatively large spin stiffnesses. Crudely, the large mass heavy-hole band dominates the spin susceptibility and enables local magnetic order at high temperatures, while the dispersive light-hole band dominates the spin stiffness and enables

long-range magnetic order. The multiband character of the semiconductor valence band plays an important role in the ferromagnetism of these materials.

Closed symbols in Fig. 1 summarize critical temperature estimates that include both the Stoner enhancement of T_c and the suppression due to spin-wave fluctuations. The data were calculated using the six-band Kohn-Luttinger model for hole densities up to one hole per Mn_{Ga} and Mn_{Ga} concentrations $x=5\%$, 8%, and 10%. Given the qualitative nature of these T_c estimates we can conclude that T_c will remain roughly proportional to x even at large dopings. The suppression of T_c due to spin waves increases with increasing hole density relative to the local moment concentration, resulting in saturation of the critical temperature with increasing p at about 50% compensation.

E. Mn_{Ga} and Mn_I partial concentrations

In the previous sections we have considered Mn to occupy only the Ga substitutional positions and found that T_c should increase linearly with the concentration of Mn_{Ga} local moments. In real (Ga,Mn)As materials a fraction of Mn is incorporated during the growth in interstitial positions. These donor impurities are likely to form pairs with Mn_{Ga} acceptors in as-grown systems with approximately zero net moment,[8,37,38] resulting in an effective free local-moment doping $x_{eff}=x_s-x_i$. Here x_s and x_i are partial concentrations of substitutional and interstitial Mn, respectively. Although Mn_I can be removed by low-temperature annealing, x_{eff} will remain smaller than the total nominal Mn doping. The Mn_{Ga} doping efficiency is, therefore, one of the key parameters that may limit maximum T_c achieved in (Ga,Mn)As epilayers.

In this section, we calculate cohesion energy $E_c(x_s,x_i)$ as a function of the partial concentrations x_s and x_i and we use it to determine the dependence of x_s and x_i on the total Mn doping in as-grown materials. We define $E_c(x_s,x_i)$ as a difference of the crystal energy per unit cell and a properly weighted sum of energies of isolated constituent atoms. The cohesion energy is not very sensitive to the details of the electronic structure and can be calculated with a reasonable accuracy, for example, by using the microscopic TBA model. Note that the growth kinetics calculations[55] identified adsorption pathways for Mn_I formation in (Ga,Mn)As epilayers. Our equilibrium consideration provides, as seen in Sec. III B, a very good estimate for the fraction of Mn impurities incorporated in interstitial positions.

The partial Mn concentrations x_s and x_i can be obtained by minimizing $E_c(x_s,x_i)$ at fixed Mn concentration $x=x_s+x_i$, with respect to either x_s or x_i. Formally, the condition for a dynamical equilibrium between the two positions of Mn has a form

$$\frac{\partial E_c(x_s,x_i)}{\partial x_s}-\frac{\partial E_c(x_s,x_i)}{\partial x_i}=0. \tag{13}$$

It was recently shown[56] that the partial derivatives of the cohesion energy $E_c(x_s,x_i)$ with respect to x_s and x_i represent formation energies F_s and F_i of Mn_{Ga} and Mn_I impurities, respectively, assuming that the atomic reservoir is formed by neutral isolated atoms. The equilibrium distribution of Mn_{Ga} and Mn_I is therefore reached when

$$F_s(x_s,x_i)=F_i(x_s,x_i), \tag{14}$$

as expected also from the growth point of view. Partial concentrations $x_{s,i}$ of Mn can be obtained by solving Eq. (13) together with the condition $0\leqslant x_{s,i}\leqslant x$, $x_s+x_i=x$.

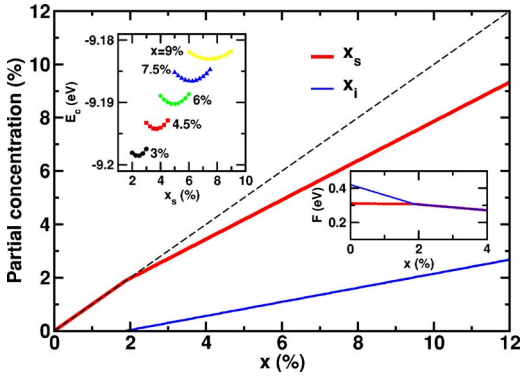

FIG. 3. (Color online) Main panel: Theoretical equilibrium partial concentrations of substitutional Mn_{Ga} (red thick line) and interstitial Mn_I (blue thin line) impurities. Right inset: Formation energies of Mn_{Ga} and Mn_I as a function of total Mn concentration. Left inset: Cohesion energy as a function of substitutional Mn_{Ga} concentration at several fixed total Mn concentrations.

The left inset of Fig. 3 summarizes the compositional dependence of the cohesion energy in (Ga,Mn)As with both Mn_{Ga} and Mn_I impurities. We consider several values of x and plot $E_c(x_s,x-x_s)$ vs x_s. Although the changes of the cohesion energy due to the incorporation of Mn are small, a systematic linear shift of the minimum of E_c with increasing x is clearly visible. Correspondingly, the partial concentration of $x_{s,i}$ is expected to increase with increasing x. For $x>1.5\%$ we obtain $x_s\approx 0.8x$ and $x_i\approx 0.2x$, in good agreement with the density-functional results.[34]

The linear relations between x_s, x_i, and x reflect the fact that the difference of the formation energies of Mn_{Ga} and Mn_I impurities (see right inset of Fig. 3) can be, up to $x=10\%$, approximated by a linear function of x_s and x_i,

$$\Delta(x_s,x_i)\equiv F_s(x_s,x_i)-F_i(x_s,x_i)\approx -0.1+5.9x_s-15.1x_i(\mathrm{eV}). \tag{15}$$

This relation allows us to interpret the theoretical distribution of Mn atoms between substitutional and interstitial sites. For $x<1.5\%$, Mn_{Ga} has a lower formation energy than Mn_I and Mn atoms tend to occupy substitutional positions. At $x\approx 1.5\%$, $\Delta(x_s,x_i)$ approaches zero and both Mn_{Ga} and Mn_I are formed with a similar probability, as shown in Fig. 3.

We note that both Mn_{Ga} and Mn_I positions remain metastable in the whole concentration range shown in Fig. 3 and that our results correspond to the as-grown rather than to the annealed materials. During the growth, the formation energies [namely, $\Delta(x_s,x_i)$] control incorporation of Mn atoms assuming that the total amount of Mn in the material is related to a sufficiently high chemical potential in the Mn source. The annealing processes, on the other hand, do not

depend on formation energies but rather on energy barriers surrounding individual metastable positions of Mn in the lattice. The barriers are larger for Mn_{Ga} (Refs. 38 and 55) so that the post-grown low-temperature annealing can be used to remove Mn_I without changing the number of Mn_{Ga} significantly.

F. Hole density and Hall coefficient

As discussed above, the level of compensation is one of the key parameters that determines Curie temperatures in (Ga,Mn)As. In this paper, as well as in a number of other experimental works, hole densities are obtained from Hall measurements. In order to estimate the uncertainty of this experimental technique we analyze in this section theoretical Hall factors, $r_H=(\rho_{xy}-\rho_{xy,0})/(B/ep)$, in ferromagnetic (Ga,Mn)As epilayers. Here $\rho_{xy,0}$ is the Hall resistivity at field $B=0$ which can be nonzero due to the anomalous Hall effect.

Detailed microscopic calculations in nonmagnetic p-type GaAs with hole densities $p\sim 10^{17}-10^{20}$ cm^{-3} showed that r_H can vary between 0.87 and 1.75, depending on doping, scattering mechanisms, and on the level on which the complexity of the GaAs valence band is modeled.[57] Here we focus on estimating the effect on r_H of the spin-splitting of the valence band and of the anomalous Hall term that is particularly large in ferromagnetic (Ga,Mn)As.

The calculations are based on numerical evaluation of the Kubo formula at finite magnetic fields. We assume band- and wave-vector-independent quasiparticle lifetimes for simplicity. It is essential for our analysis to allow for both intraband and interband transitions. At zero magnetic field, the interband transitions between SO-coupled, spin-split bands give rise to the anomalous Hall effect (AHE), i.e., to a nonzero ρ_{xy} that is proportional to the magnetization.[58] On the other hand, the ordinary Hall resistance, which is proportional to B, arises, within the simple single-band model, from intraband transitions between adjacent Landau levels. The Kubo formula that includes both intraband and interband transitions allows us to capture simultaneously the anomalous and ordinary Hall effects in the complex (Ga,Mn)As valence bands.

Many of the qualitative aspects of the numerical data shown in Figs. 4 and 5 can be explained using a simple model of a conductor with two parabolic uncoupled bands. Note that the typical scattering rate in (Ga,Mn)As epilayers is $\hbar/\tau\sim 100$ meV and the cyclotron energy at $B=5$ T is $\hbar\omega\sim 1$ meV, i.e., the system is in the strong scattering limit, $\omega\tau\ll 1$. In this limit, the two band model gives resistivities:

$$\rho_{xx}\approx\frac{1}{\sigma_{xx,1}+\sigma_{xx,2}}\approx\frac{1}{\sigma_{0,1}+\sigma_{0,2}}$$

$$\rho_{xy}\approx-\frac{\sigma_{xy,1}+\sigma_{xy,2}}{(\sigma_{xx,1}+\sigma_{xx,2})^2}=\frac{B}{ep_1}\frac{1+\frac{p_2}{p_1}\left(\frac{m_1^*}{m_2^*}\right)^2}{\left(1+\frac{p_2}{p_1}\frac{m_1^*}{m_2^*}\right)^2}\geqslant\frac{B}{ep},\quad(16)$$

where the indices 1 and 2 correspond to the first and second band, respectively, the total density $p=p_1+p_2$, and the zero-field conductivity $\sigma_0=e^2\tau p/m^*$. Equation (16) suggests that in the strong scattering limit the multiband nature of the hole states in (Ga,Mn)As should not result in a strong longitudinal magnetoresistance. This observation is consistent with the measured weak dependence of ρ_{xx} on B for magnetic fields at which magnetization in the (Ga,Mn)As ferromagnet is saturated.[59]

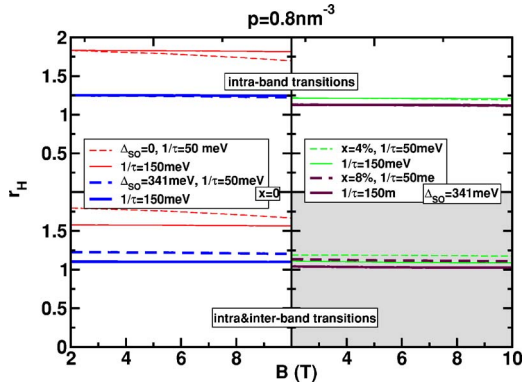

FIG. 4. (Color online) Theoretical Hall factors for $p=0.8$ nm^{-3}; $\hbar/\tau=50$ meV (dashed lines), $\hbar/\tau=150$ meV (solid lines). Top panels: only intraband transitions are taken into account. Bottom panels: intraband and interband transitions are taken into account. Left panels: GaAs ($x=0$); zero SO coupling (thin lines), $\Delta_{SO}=341$ meV (thick lines). Right panels: (Ga,Mn)As with Mn_{Ga} concentration 4% (thin lines), 8% (thick lines). $\rho_{xy}=0$ in all panels except for the bottom left panel where $\rho_{xy}(B=0)\neq 0$ due to the anomalous Hall effect.

The simple two-band model also suggests that the Hall factor r_H is larger than 1 in multiband systems with different dispersions of individual bands. Indeed, for uncoupled valence bands, i.e., when accounting for intraband transitions only, the numerical Hall factors in the top panels of Figs. 4 and 5 are larger than 1 and independent of τ as also suggested by Eq. (16). The suppression of r_H when SO coupling is turned on, shown in the same graphs, results partly from depopulation of the angular momentum $j=\frac{1}{2}$ split-off bands. In addition to this "two-band model"–like effect, the inter-Landau-level matrix elements are reduced due to SO coupling since the spinor part of the eigenfunctions now varies

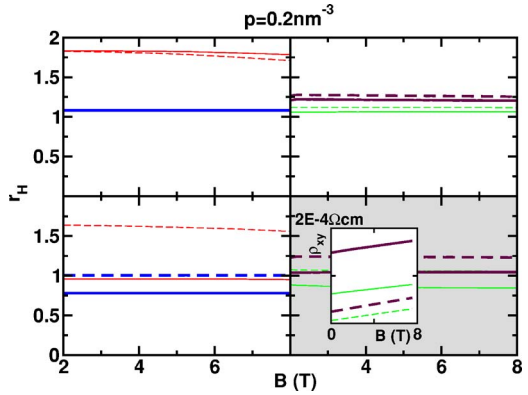

FIG. 5. (Color online) Theoretical Hall factors for $p=0.2$ nm^{-3}; same line coding as in Fig. 4. Inset: Theoretical Hall curves showing the anomalous Hall effect contribution at $B=0$.

with the Landau-level index. In ferromagnetic $Ga_{1-x}Mn_xAs$ the bands are spin-split and higher bands depopulated as x increases. In terms of r_H, this effect competes with the increase of the inter-Landau-level matrix elements since the spinors are now more closely aligned within a band due to the exchange field produced by the polarized Mn moments. Increasing x can therefore lead to both decrease or increase of r_H depending on other parameters of the (Ga,Mn)As, such as the hole density (compare top right panels of Figs. 4 and 5).

The interband transitions result in a more single-band-like character of the system, i.e., r_H is reduced, and the slope of the $\rho_{xy}(B)$ curve now depends more strongly on τ. Although the anomalous and ordinary Hall effect contributions to ρ_{xy} cannot be simply decoupled, the comparison of numerical data in the four panels and the inset in Fig. 5 confirms the usual assumption that the anomalous Hall effect produces a field-independent off-set proportional to magnetization and ρ_{xx}^2. The comparison also suggests that after subtracting $\rho_{xy}(B=0)$, r_H can be used to determine the hole density in (Ga,Mn)As with accuracy that is better than in nonmagnetic GaAs with comparable hole densities. For typical hole and Mn densities in experimental (Ga,Mn)As epilayers we estimate the error of the Hall measurement of p to be within ±20%.

III. EXPERIMENT

A. Measured Curie temperatures and hole densities

A series of (Ga,Mn)As thin films with varying Mn content were grown by LT-MBE using As_2. The layer structure is 25 or 50 nm(Ga,Mn)As/50-nm low-temperature GaAs/100-nm high-temperature (580 °C)GaAs/GaAs(100) substrate. For a given Mn content, the growth temperature of the (Ga,Mn)As layer and the GaAs buffer is chosen in order to minimize As antisite densities while maintaining two-dimensional growth and preventing phase segregation. We find that the growth temperature must be decreased as the Mn concentration is increased: for the lowest Mn content the growth temperature was ~300 °C, for the highest it was ~180 °C. Full details of the growth are presented elsewhere.[60,61]

The Mn content was controlled by varying the Mn/Ga incident flux ratio, measured *in situ* and calibrated using secondary-ion-mass spectroscopy (SIMS) measurements on 1 μm thick (Ga,Mn)As films, grown under otherwise identical conditions to the samples considered here. A detailed comparison of the results of a number of different calibration techniques, presented in Ref. 62, allows us to assign an uncertainty of ±10% to the quoted Mn concentrations. However, it should be noted that the SIMS measurements yield the *total* volume density of Mn in the (Ga,Mn)As films, and not the fraction of Ga substituted by Mn. This is important as it is expected that a fraction of the Mn will be incorporated on interstitial as well as substitutional sites.[3] We define the Mn concentration x as the total Mn volume density relative to the volume density of Ga in GaAs.

Hall bar structures, of width 200 μm and length 1 mm, were fabricated from the (Ga,Mn)As samples using photolithography. Simultaneous magnetoresistance and Hall effect measurements were performed using standard low-frequency ac techniques, in order to extract both the Curie temperature T_c and the hole density p, as detailed below. Magnetic fields of up to ±0.7 T and ±16.5 T were used to obtain T_c and p, respectively. Following these measurements, the samples were annealed in air at 190 °C. The electrical resistance was monitored during annealing, and the anneal was halted when this appeared to have reached a minimum (after typically 50 to 150 h). The T_c and p were then remeasured.

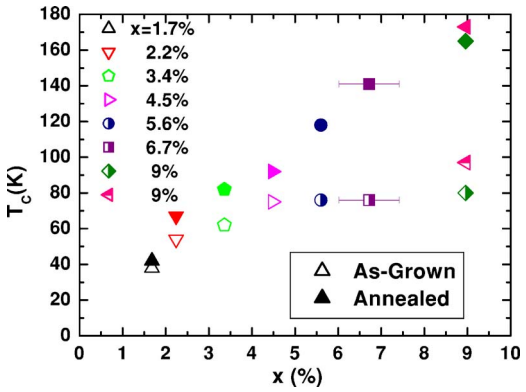

FIG. 6. (Color online) Experimental Curie temperature vs total Mn doping. T_c is measured from the anomalous Hall effect, Mn doping by SIMS. Open symbols correspond to as-grown samples, half-open symbols to as-grown samples with large charge compensation, and filled symbols to annealed samples. For clarity, error bars are shown only for the x=6.7% sample.

Below T_c, the Hall resistance R_{xy} in (Ga,Mn)As is dominated by the anomalous Hall effect, with $R_{xy} \sim R_A M_z$, where M_z is the perpendicular component of the magnetization, and the coefficient R_A is roughly proportional to the square of the resistivity, ρ_{xx}. Therefore, R_{xy}/ρ_{xx}^2 gives a direct measurement of M_z, which can be used to extract T_c using Arrot plots.[63] The value of T_c obtained depends only weakly on the precise dependence of R_A on ρ_{xx} assumed, since ρ_{xx} varies only slowly close to T_c, while R_{xy} varies rapidly. We are therefore able to obtain T_c within an accuracy of ±1 K by this method.[59]

T_c obtained for the (Ga,Mn)As Hall bar samples before and after annealing are shown vs x in Fig. 6. It can be seen that the low-temperature annealing procedure results in a marked increase in T_c as has been found previously.[64] Increases of T_c by more than a factor of 2 are possible. This effect becomes larger as the Mn concentration increases. Since the T_c enhancement is associated with out-diffusion and passivation of interstitial Mn,[8] this indicates that as the incident Mn flux is increased, an increasing fraction is incorporated on interstitial sites, as predicted in Sec. II E.

To obtain hole densities from R_{xy}, it is necessary to separate the small normal Hall term from the much larger anomalous Hall term. Measurements were performed at 0.3 K and in magnetic fields above 10 T, i.e., under conditions where the normal Hall term gives the dominant field-dependent contribution to R_{xy}. Then, the measured R_{xy} was fitted to $(\alpha\rho^2 + r_H B)$, where ρ_{xx} and B are the measured resistivity and magnetic field, and α and r_H are fit parameters. Finally, the

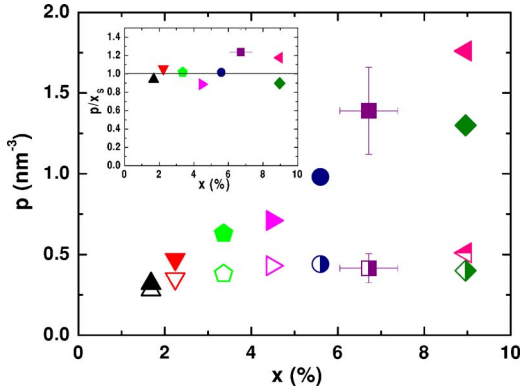

FIG. 7. (Color online) Experimental hole density vs total Mn doping. Hole density is measured by ordinary Hall effect. Same symbol coding is used as in Fig. 6.

hole density is obtained from $r_H=1/(pew)$, where w is the (Ga,Mn)As layer thickness. From the detailed calculations described in Sec. II F we can ascribe an uncertainty of ±20% to the values of p obtained using this method. The measured p for the (Ga,Mn)As Hall bar samples before and after annealing are shown vs x in Fig. 7. We see that annealing greatly increases p for large x. Data in the inset of Fig. 7, discussed in detail in Sec. III B, show that within error the samples are uncompensated after annealing.

B. Substitutional and interstitial Mn

From the measured hole density p before and after annealing, and the total Mn density x, values can be obtained for the density of incorporated Mn occupying acceptor substitutional and double donor interstitial lattice sites, x_s and x_i. These are obtained using the following assumptions: (i) the only contribution to the total Mn density determined by SIMS are from substitutional and interstitial Mn, i.e., $x=x_s+x_i$; (ii) the only source of compensation in the (Ga,Mn)As films are the interstitial Mn, which are double donors, i.e., $p=4/a_{lc}^3(x_s-2x_i)$; (iii) the low-temperature annealing procedure affects only x_i, and not x_s. The values of x_s and x_i in the unannealed films obtained under these assumptions are shown in Fig. 8. We find a remarkably good agreement between experiment and the theoretical TBA/CPA data from Sec. II E and *ab initio* results.[34] As a consistency check, we show in the inset of Fig. 7 the ratio of hole density to substitutional Mn_{Ga} density after annealing, as obtained under the above assumptions. Within the experimental error we obtain one hole per substitutional Mn_{Ga} after annealing, that is, there is no significant compensation in the annealed (Ga,Mn)As films. This justifies our neglect of additional compensating defects such as As_{Ga} in determining x_s and x_i.

C. T_c vs Mn_{Ga}, effective Mn_{Ga}, and hole densities

Since we obtain reasonably accurate values for T_c, hole densities and the partial Mn_{Ga} and Mn_I concentrations for the set of samples considered here, we now attempt to assess on the basis of the experimental data the key factors determining T_c and to compare the experimental results with the broad predictions of theory.

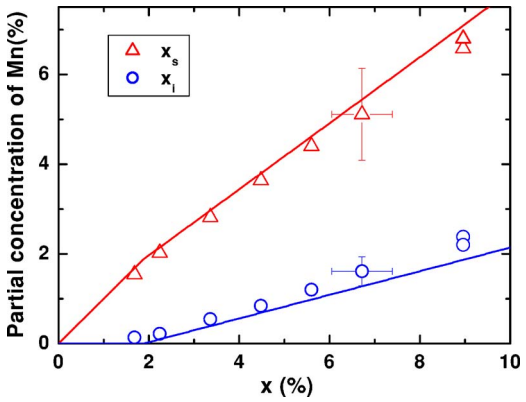

FIG. 8. (Color online) Experimental partial concentrations of Mn_{Ga} (triangles) and Mn_I (circles) in as-grown samples. Data show no saturation of Mn_{Ga} with increasing total Mn doping consistent with theory expectation (solid lines).

In Fig. 6 T_c was plotted against total Mn concentration. Before annealing the T_c values of samples with high compensation (samples with large compensation are indicated as half filled symbols in this and subsequent figures) do not increase significantly with increasing total Mn density but a steady increase is recovered after annealing. In Fig. 9 T_c is plotted against the substitutional Mn_{Ga} concentration. The form of Figs. 6 and 9 are broadly similar despite the different x axes. We expect, however, and will assume in the following discussion that any Mn_I donor present is attracted to a Mn_{Ga} acceptor and that the pair couples antiferromagnetically.[38] Then the effective uncompensated moment density will be $x_{eff}=x_s-x_i$. Plotting T_c against x_{eff} in Fig. 10 reveals that for all the low compensation samples T_c increases approximately linearly with x_{eff} but that as compensation, $(1-pa_{lc}^3/4x_{eff})$, increases above ~40% the measured T_c values fall increasingly far below this linear trend.

If T_c is plotted against hole density, as is done in the inset of Fig. 11, it is found to increase monotonically. However, this is primarily due to the increase in hole density with x_{eff}. The main plot in Fig. 11 shows that T_c/x_{eff} is almost inde-

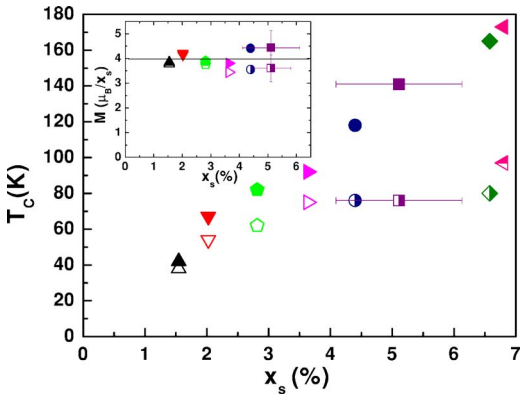

FIG. 9. (Color online) Experimental T_c vs Mn_{Ga} concentration, x_s (see text for definition of x_s). Magnetization per x_s is shown in the inset.

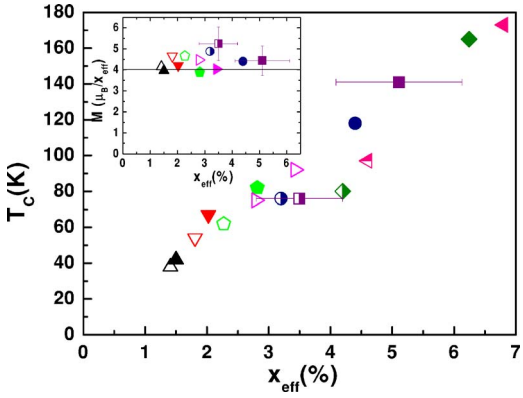

FIG. 10. (Color online) Experimental T_c vs effective Mn_{Ga} concentration, x_{eff} (see text for definition of x_{eff}). Magnetization per x_{eff} is shown in the inset.

pendent of hole density except for the case of the high compensation samples which clearly stand out as showing different behavior.

To compare with the predictions of Sec. II, we finally plot T_c/x_{eff} against p/N_{Mn}^{eff} in Fig. 12, where $N_{\mathrm{Mn}}^{eff}=4x_{eff}/a_{lc}^3$. We emphasize here that a precise comparison between theory and experiment is not meaningful as the modeling techniques do not allow us to capture the complexities of ferromagnetic states in (Ga,Mn)As on a fully quantitative level, as explained in the Introduction. On the other hand, all experimental points in Fig. 12 show a common T_c trend which is consistent with the theoretical models discussed in Sec. II and the magnitudes of the experimental and calculated T_c/x_{eff} are also comparable. Further confirmation of the theoretical picture is seen from the very weak experimental dependence of T_c/x_{eff} on p/N_{Mn}^{eff} for low compensation and the relatively rapid fall of T_c/x_{eff} with decreasing p/M_{Mn}^{eff} for compensations of ~40% or larger.

As a consistency check for considering x_{eff} as the density of local Mn_{Ga} moments participating in the ordered ferromagnetic state, magnetization data are shown in insets of Figs. 9 and 10. Magnetizations were determined by superconducting quantum interference device magnetometry, at a sample temperature of 5 K, and using an external field of

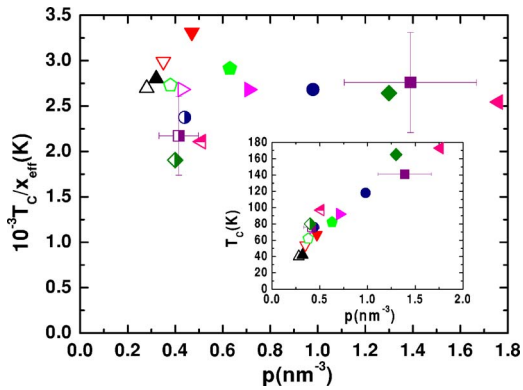

FIG. 11. (Color online) Experimental T_c/x_{eff} vs hole density. T_c/x_{eff} is nearly independent of hole density except in highly compensated samples. Inset: T_c vs hole density.

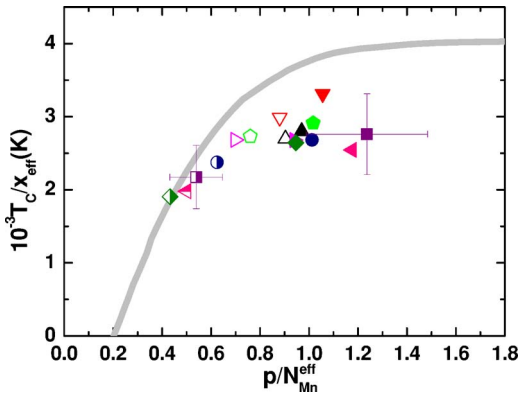

FIG. 12. (Color online) Experimental T_c/x_{eff} vs hole density relative to effective concentration of Mn_{Ga} moments. Deviation from linear dependence on x_{eff} are seen only for high compensations $(1-pa_{lc}^3/4x_{eff}>40\%)$ in agreement with theory. For weakly compensated samples T_c shows no signs of saturation with increasing x_{eff}. Theoretical (gray) T_c trend from Fig. 2 is plotted for comparison.

0.3 T to overcome in-plane anisotropy fields. The charge and moment compensation after annealing is not significant for our samples and the moment per x_s or x_{eff} is around $\sim 4\mu_B - 4.5\mu_B$. This corresponds within the error bars to the $5\mu_B$ contribution of the $S=\frac{5}{2}$ local Mn_{Ga} moment and $\sim(-0.25)-(-0.5)\mu_B$ contribution of the antiferromagnetically coupled valence-band hole[25] in collinear (Ga,Mn)As ferromagnets. In the inset of Fig. 9 we see that the measured moment per x_s are all below $4\mu_B$ for the compensated samples. Including the effects of the Mn_I—Mn_{Ga} antiferromagnetic coupling by considering the moment per x_{eff} reveals again values around $4.5\mu_B$. Our conclusion, therefore, is that if we assume no significant frustration in our samples and account for the antiferromagnetic Mn_I—Mn_{Ga} coupling, our extensive set of T_c, hole density, Mn density, and magnetization data brings up a clear common picture of T_c trends in the 16 different (Ga,Mn)As ferromagnetic semiconductors we have studied, that is consistent with the theory predictions summarized in Sec. II.

IV. DISCUSSION

The preceding considerations of the factors determining T_c in (Ga,Mn)As lead us to conclude that there are no fundamental physics barriers to achieving room temperature ferromagnetism in this system. Experimental results for T_c in samples in which compensating defects other than interstitial Mn have been reduced to very low levels have been shown to be in good agreement with theoretical expectations. Moment compensation by interstitial Mn_I impurities becomes increasingly important as the concentration of total Mn is increased. However, for the range of total Mn concentrations considered experimentally we find that the level of substitutional Mn_{Ga} continues to increase with x. Furthermore low-temperature post-growth annealing is found to effectively remove Mn_I in thin film samples even at large x, leading to material which within experimental error is both charge and

moment uncompensated. Most importantly for samples in which the charge compensation is less than ~40%, we find theoretically and experimentally that T_c increases approximately linearly with effective concentration x_{eff} of Mn_{Ga}, whose moments are not compensated by near-neighbor Mn_I impurities. We have not observed any signs of saturation in this trend in the studied (Ga,Mn)As diluted magnetic semiconductors. It should be noted that our maximum x_{eff} is only 4.6% in the as grown sample and 6.8% after annealing for a total Mn concentration $x=9\%$; hence the modest T_c's observed so far. Achieving T_c values close to room temperature in (Ga,Mn)As, which we expect to occur for $x_{eff} \approx 10\%$ is essentially a technological issue, albeit a very challenging one. In the remaining paragraphs of this section we discuss these challenges in more detail.

Low-temperature MBE growth is used to achieve levels of Mn incorporation in (Ga,Mn)As far in excess of the equilibrium solubility level. When growing (Ga,Mn)As with Mn concentrations of several percent it is known that the Mn tends to accumulate on the surface[60,61] in a similar way to all high vapor pressure dopants in GaAs and to the higher vapor pressure species, e.g. In in $In_xGa_{1-x}As$. For homogenous Mn incorporation during continuous growth, a surface Mn concentration is required that is higher than the bulk concentration. For a given Mn concentration this density gradient is temperature dependent, increasing with increasing temperature. This leads to an upper temperature limit for successful growth when the Mn surface concentration approaches a significant proportion of a monolayer, after which point surface clustering of Mn occurs, frustrating the growth.[60,61] Furthermore, higher Mn fluxes require lower growth temperatures.

The pursuit of higher Curie temperatures has driven growth efforts to very low temperatures compared with conventional MBE of GaAs. In this regime (~200–250 °C) significant levels of compensating defects such as As_{Ga} and vacancies usually occur in GaAs.[65] The density of As_{Ga} defects can be reduced by close to stoichiometric growth with As_2,[66] requiring very precise control over the As flux.

Apart from precise control over the stoichiometry and the attendant requirement for flux stability, a major technical difficulty arises from the measurement and control of the growth temperature. In order to measure substrate temperature, most MBE machines in use today employ a thermocouple heated by radiation from the substrate or substrate holder. At normal growth temperatures (~580 °C) the radiant flux from the substrate is high and the relationship between substrate and thermocouple is repeatable with a short time constant, allowing for good temperature stability and control. At low temperatures, however, the radiant flux between the substrate and thermocouple is low, leading to a heightened sensitivity to local conditions such as holder emissivity, radiant heat from the metal sources, shutter transients etc., and also long time constants. This significantly increases the error in the temperature measurement as well as the likelihood of temperature spikes and drift as shutters are opened and growth proceeds. In MBE, optical pyrometers are ubiquitous as secondary temperature calibration devices but most cannot read accurately at these low temperatures and in many common configurations suffer from potential inaccuracies due to reflection off the Knudsen cells if used during growth.

It is desirable to grow at as high temperature as possible for a given Mn flux, while maintaining two-dimensional (2D) growth and avoiding Mn clustering. However, with such large errors and potential temperature drift, growers tend to err toward lower than ideal temperatures in order to sustain the growth. To explore fully the parameter space, effort should be directed toward improving the control of both metal fluxes and substrate temperature. This will maximize the chances of increasing the doping towards the 10% Mn_{Ga}, required for room temperature ferromagnetism. The increases in T_c achieved in the last few years lead us to believe that higher transition temperatures will be obtained using conventional MBE. Growth interrupt strategies such as migration enhanced epitaxy[67] may have advantages over conventional MBE for the incorporation of higher levels of substitutional Mn, however, they will be especially sensitive to poor temperature stability and shutter transients and so they will require even more precise temperature control.

V. CONCLUSION

Based on the broad agreement between theoretical and experimental Curie temperature trends in (Ga,Mn)As with Mn concentrations larger than 1.5% we can outline the following strategies for achieving room temperature ferromagnetism in this semiconductor.

(i) T_c increases linearly with the concentration x_{eff} of local Mn_{Ga} moments participating in the ordered ferromagnetic state. Room temperature ferromagnetism should be achieved at $x_{eff} \approx 10\%$. Interstitial Mn_I impurities reduce the number of these ordered Mn_{Ga} moments due to the strong antiferromagnetic Mn_{Ga}—Mn_I near-neighbor coupling. Mn_I, however, can be efficiently removed by post-growth annealing.

(ii) Equilibrium considerations, confirmed experimentally in samples with Mn_{Ga} concentrations up to 6.8%, suggest that there is no fundamental physics barrier for increasing Mn_{Ga} concentration to and beyond 10%. A very precise control over the growth temperature and stoichiometry is, however, required for maintaining the 2D growth mode of the high quality, uniform (Ga,Mn)As materials.

(iii) Ferromagnetic coupling between the ordered local Mn_{Ga} moments is mediated by itinerant holes. For charge compensations $(1-pa_{lc}^3/4x_{eff}) > 40\%$, the Curie temperature falls down with decreasing p. At compensations smaller than ~40%, however, T_c is almost independent of the hole density. A modest charge compensation is, therefore, not an important limiting factor in the search of high Curie temperature ferromagnetic semiconductors based on (Ga,Mn)As and may be desirable to maximize the possibilities for doping and gate control of ferromagnetism.

ACKNOWLEDGMENTS

We acknowledge support from the Grant Agency of the Czech Republic through Grant No. 202/05/0575 from the Academy of Sciences of the Czech Republic through Insti-

tutional Support No. AV0Z10100521, from the Ministry of Education of the Czech Republic through the Center for Fundamental Research LC510, from the EU FENIKS Project No. EC:G5RD-CT-2001-00535, the support from the UK EPSRC through Grant No. GR/S81407/01, from the Welch Foundation, the Department of Energy under Grant No. DE-FG03-02ER45958, and from Deutsche Forschungsgemeinschaft through Grant No. SFB 491.

[1] H. Ohno, Science **281**, 951 (1998).
[2] S. J. Potashnik, K. C. Ku, R. Mahendiran, S. H. Chun, R. F. Wang, N. Samarth, and P. Schiffer, Phys. Rev. B **66**, 012408 (2002).
[3] K. M. Yu, W. Walukiewicz, T. Wojtowicz, I. Kuryliszyn, X. Liu, Y. Sasaki, and J. K. Furdyna, Phys. Rev. B **65**, 201303(R) (2002).
[4] K. M. Yu, W. Walukiewicz, T. Wojtowicz, W. L. Lim, X. Liu, U. Bindley, M. Dobrowolska, and J. K. Furdyna, Phys. Rev. B **68**, 041308(R) (2003).
[5] K. Edmonds, K. Wang, R. Campion, A. Neumann, N. Farley, B. Gallagher, and C. Foxon, Appl. Phys. Lett. **81**, 4991 (2002).
[6] D. Chiba, K. Takamura, F. Matsukura, and H. Ohno, Appl. Phys. Lett. **82**, 3020 (2003).
[7] K. C. Ku, S. J. Potashnik, R. F. Wang, M. J. Seong, E. Johnston-Halperin, R. C. Meyers, S. H. Chun, A. Mascarenhas, A. C. Gossard, D. D. Awschalom, P. Schiffer, and N. Samarth, Appl. Phys. Lett. **82**, 2302 (2003).
[8] K. Edmonds, P. Boguslawski, K. Wang, R. Campion, N. Farley, B. Gallagher, C. Foxon, M. Sawicki, T. Dietl, M. Nardelli, and J. Bernholc, Phys. Rev. Lett. **92**, 037201 (2004).
[9] K. Wang, R. Campion, K. Edmonds, M. Sawicki, T. Dietl, C. Foxon, and B. Gallagher, AIP Conf. Proc. **772**, 333 (2005).
[10] M. B. Stone, K. C. Ku, S. J. Potashnik, B. L. Sheu, N. Samarth, and P. Schiffer, Appl. Phys. Lett. **83**, 4568 (2003).
[11] T. Jungwirth, W. A. Atkinson, B. H. Lee, and A. H. MacDonald, Phys. Rev. B **59**, 9818 (1999).
[12] T. Dietl, H. Ohno, F. Matsukura, J. Cibert, and D. Ferrand, Science **287**, 1019 (2000).
[13] T. Jungwirth, J. König, J. Sinova, J. Kučera, and A. H. MacDonald, Phys. Rev. B **66**, 012402 (2002).
[14] L. Brey and G. Gómez-Santos, Phys. Rev. B **68**, 115206 (2003).
[15] S. Das Sarma, E. H. Hwang, and D. J. Priour, Jr., Phys. Rev. B **70**, 161203(R) (2004).
[16] L. M. Sandratskii and P. Bruno, Phys. Rev. B **66**, 134435 (2002).
[17] K. Sato, P. H. Dederichs, and H. Katayama-Yoshida, Europhys. Lett. **61**, 403 (2003).
[18] L. M. Sandratskii, P. Bruno, and J. Kudrnovský, Phys. Rev. B **69**, 195203 (2004).
[19] S. Hilbert and W. Nolting, Phys. Rev. B **71**, 113204 (2005).
[20] T. Jungwirth, J. Mašek, J. Sinova, and A. H. MacDonald, Phys. Rev. B **68**, 161202(R) (2003).
[21] C. Timm, J. Phys.: Condens. Matter **15**, R1865 (2003).
[22] I. Vurgaftman, J. Meyer, and L. Ram-Mohan, J. Appl. Phys. **89**, 5815 (2001).
[23] J. Okabayashi, A. Kimura, O. Rader, T. Mizokawa, A. Fujimori, T. Hayashi, and M. Tanaka, Phys. Rev. B **58**, R4211 (1998).
[24] T. Omiya, F. Matsukura, T. Dietl, Y. Ohno, T. Sakon, M. Motokawa, and H. Ohno, Physica E (Amsterdam) **7**, 976 (2000).
[25] T. Dietl, H. Ohno, and F. Matsukura, Phys. Rev. B **63**, 195205 (2001).
[26] M. Abolfath, T. Jungwirth, J. Brum, and A. H. MacDonald, Phys. Rev. B **63**, 054418 (2001).
[27] M. Sawicki, F. Matsukura, A. Idziaszek, T. Dietl, G. M. Schott, C. Ruester, C. Gould, G. Karczewski, G. Schmidt, and L. M. Molenkamp, Phys. Rev. B **70**, 245325 (2004).
[28] M. Sawicki, K.-Y. Wang, K. W. Edmonds, R. Campion, C. Staddon, N. Farley, C. Foxon, E. Papis, E. Kaminska, A. Piotrowska, T. Dietl, and B. L. Gallagher, Phys. Rev. B **71**, 121302(R) (2005).
[29] T. Jungwirth, J. Sinova, K. Wang, K. W. Edmonds, R. Campion, B. Gallagher, C. Foxon, Q. Niu, and A. H. MacDonald, Appl. Phys. Lett. **83**, 320 (2003).
[30] H. X. Tang, R. K. Kawakami, D. D. Awschalom, and M. L. Roukes, Phys. Rev. Lett. **90**, 107201 (2003).
[31] C. Gould, C. Rüster, T. Jungwirth, E. Girgis, G. M. Schott, R. Giraud, K. Brunner, G. Schmidt, and L. W. Molenkamp, Phys. Rev. Lett. **93**, 117203 (2004).
[32] A. Giddings, M. Khalid, T. Jungwirth, J. Wunderlich, S. Yasin, R. Campion, K. Edmonds, J. Sinova, K. Ito, K. Y. Wang, D. Williams, B. L. Gallagher, and C. T. Foxton, Phys. Rev. Lett. **94**, 127202 (2005).
[33] J. König, T. Jungwirth, and A. H. MacDonald, Phys. Rev. B **64**, 184423 (2001).
[34] J. Mašek, I. Turek, J. Kudrnovský, F. Máca, and V. Drchal, Acta Phys. Pol. A **105**, 637 (2004).
[35] F. Máca and J. Mašek, Phys. Rev. B **65**, 235209 (2002).
[36] J. Kudrnovský, I. Turek, V. Drchal, J. Mašek, F. Máca, and P. Weinberger, J. Supercond. **16**, 119 (2003).
[37] J. Blinowski and P. Kacman, Phys. Rev. B **67**, 121204(R) (2003).
[38] J. Mašek and F. Máca, Phys. Rev. B **69**, 165212 (2003).
[39] D. E. Bliss, W. Walukiewicz, J. W. Ager, III, E. E. Haller, K. T. Chan, and S. Tanigawa, J. Appl. Phys. **71**, 1699 (1992).
[40] R. P. Campion, K. W. Edmonds, L. X. Zhao, K. Y. Wang, C. T. Foxon, B. L. Gallagher, and C. R. Staddon, J. Cryst. Growth **251**, 311 (2003).
[41] J. Kudrnovský, I. Turek, V. Drchal, F. Máca, P. Weinberger, and P. Bruno, Phys. Rev. B **69**, 115208 (2004).
[42] T. Dietl, A. Haury, and Y. M. d'Aubigne, Phys. Rev. B **55**, R3347 (1997).
[43] J. König, J. Schliemann, T. Jungwirth, and A. MacDonald, in *Electronic Structure and Magnetism of Complex Materials*, edited by D. Singh and D. Papaconstantopoulos (Springer-Verlag, Berlin, 2003); cond-mat/0111314 (unpublished).
[44] C. Timm and A. H. MacDonald, Phys. Rev. B **71**, 155206 (2005).
[45] G. A. Fiete, G. Zaránd, B. Jankó, P. Redliński, and C. P. Moca, Phys. Rev. B **71**, 115202 (2005).
[46] P. Mahadevan and A. Zunger, Appl. Phys. Lett. **85**, 2860 (2004).
[47] D. N. Talwar and C. S. Ting, Phys. Rev. B **25**, 2660 (1982).
[48] W. Harrison, *Electronic Structure and the Properties of Solid* (Freeman, San Francisco, 1980).
[49] T. Jungwirth, M. Abolfath, J. Sinova, J. Kučera, and A. MacDonald, Appl. Phys. Lett. **81**, 4029 (2002).
[50] J. Mašek, Solid State Commun. **78**, 351 (1991).

[51] J. K. Furdyna, J. Appl. Phys. **64**, R29 (1988).
[52] J. Schliemann, J. König, and A. H. MacDonald, Phys. Rev. B **64**, 165201 (2001).
[53] J. Schliemann, J. König, H. Lin, and A. MacDonald, Appl. Phys. Lett. **78**, 1550 (2001).
[54] J. König, H. H. Lin, and A. H. MacDonald, Phys. Rev. Lett. **84**, 5628 (2000).
[55] S. C. Erwin and A. G. Petukhov, Phys. Rev. Lett. **89**, 227201 (2002).
[56] J. Mašek, I. Turek, V. Drchal, J. Kudrnovský, and F. Máca, Acta Phys. Pol. A **102**, 673 (2002); cond-mat/0302176 (unpublished).
[57] B. W. Kim and A. Majerfeld, Prog. Oceanogr. **17**, 17 (1995).
[58] J. Sinova, T. Jungwirth, and J. Černe, Int. J. Mod. Phys. B **18**, 1083 (2004).
[59] K. W. Edmonds, K. Y. Wang, R. P. Campion, A. C. Neumann, C. T. Foxon, B. L. Gallagher, and P. C. Main, Appl. Phys. Lett. **81**, 3010 (2002).
[60] R. Campion, K. Edmonds, L. Zhao, K. Wang, C. Foxon, B. Gallagher, and C. Staddon, J. Cryst. Growth **247**, 42 (2003).
[61] C. T. Foxon, R. P. Campion, K. W. Edmonds, L. Zhao, K. Wang, N. R. S. Farley, C. R. Staddon, and B. L. Gallagher, J. Mater. Sci. **15**, 727 (2004).
[62] L. X. Zhao, R. P. Campion, P. F. Fewster, R. W. Martin, B. Y. Ber, A. P. Kovarsky, C. R. Staddon, K. Y. Wang, K. W. Edmonds, C. T. Foxon, and B. L. Gallagher, Semicond. Sci. Technol. **20**, 369 (2005).
[63] F. Matsukura, H. Ohno, A. Shen, and Y. Sugawara, Phys. Rev. B **57**, R2037 (1998).
[64] T. Hayashi, Y. Hashimoto, S. Katsumoto, and Y. Iye, Appl. Phys. Lett. **78**, 1691 (2001).
[65] D. Hurle, J. Appl. Phys. **85**, 6957 (1999).
[66] M. Missous and K. E. Singer, Appl. Phys. Lett. **50**, 694 (1987).
[67] J. Sadowski, R. Mathieu, P. Svedlindh, M. Karlsteen, J. Kanski, L. Ilver, H. Åsklund, K. Swiatek, J. Z. DomagaIa, J. Bak-Misiuk, and D. Maude, Physica E (Amsterdam) **10**, 181 (2001).